Fig. 9. La bocca della verita: Vassili I. Moroz (*33*).

by CO_2 within the volatile inventory: OMEGA found no definite evidence that CO_2 sustained a long-term greenhouse effect enabling liquid H_2O to remain stable at the surface of Mars in the post-Noachian terrains. The OMEGA observations to date are consistent with an early escape of most of the Mars atmosphere, leaving the atmosphere as the major present CO_2 reservoir; water has been found trapped in two sinks: as ice mixed with dust within the two large perennial polar caps and as surface hydrated minerals, which seem to have been synthesized during the early evolution of Mars.

If indeed the water remained essentially stable in solid and gaseous states during the past 3 billion years, with only transient episodes of liquid water brought to the surface, then the episodic evolution of the obliquity (*29*) might have played a major role in the observed surface composition: in condensing water ice in a variety of areas determined by the atmospheric circulation in different insolation conditions, resulting in morphological and compositional (alteration) effects, that can be observed in the present surface properties of a number of areas.

References and Notes

1. J.-P. Bibring *et al.*, *Eur. Space Agency Spec. Pub.* **1240**, 37 (2004).
2. A. Chicarro, P. Martin, R. Trautner, *Eur. Space Agency Spec. Pub.* **1240**, 3 (2004).
3. J. F. Mustard *et al.*, *Science* **307**, 1594 (2005); published online 17 February 2005 (10.1126/science.1109098).
4. The Martian chronology is described in three epochs on the basis of the density of impact craters identified on optical images. The first epoch, named Noachian, corresponds to the early heavy bombardment, which ended ~3.8 billion years ago (Noachis is a region located within the highly cratered terrains, which still cover ~40% of the Mars surface, primarily in the south). The second period, or Hesperian (named after Hesperia Planitia as a typical area of this age), lasted until ~2 billion years. It is followed by the most recent Amazonian period (Amazonia Planitia belongs to the least cratered volcanic plain).
5. J. L. Bandfield, V. E. Hamilton, P. R. Christensen, *Science* **287**, 1626 (2000).
6. J. L. Bandfield, *J. Geophys. Res.* **107**, 5092 (2002).
7. V. E. Hamilton *et al.*, *Meteorit. Planet. Sci.* **38**, 871 (2003).
8. J. F. Mustard *et al.*, *J. Geophys. Res.* **102**, 25605 (1997).
9. M. B. Wyatt, H. Y. McSween, *Nature* **417**, 263 (2002).
10. M. E. Minitti *et al.*, *J. Geophys. Res.* **107**, E5 10.1029 (2002).
11. P. H. Schultz, J. F. Mustard, *J. Geophys. Res.* **109**, E01001 (2004).
12. T. M. Hoefen *et al.*, *Science* **302**, 627 (2003).
13. F. Poulet, S. Erard, *J. Geophys. Res.* **109**, E2009 (2004).
14. J.-P. Bibring *et al.*, *Nature* **428**, 627 (2004).
15. S. Byrne, A. P. Ingersoll, *Geophys. Res. Lett.* **30**, 1696 (2003).
16. Y. Langevin *et al.*, *Science* **307**, 1581 (2005); published online 17 February 2005 (10.1126/science.1109438).
17. H. H. Kieffer, T. N. Titus, *Icarus* **154**, 162 (2001).
18. A. S. Yen, S. S. Kim, M. H. Hecht, M. S. Frant, B. Murray, *Science* **289**, 1909 (1999).
19. M. S. Milliken, J. F. Mustard, *Lunar Planet. Sci. Conf.* **XXXIV**, 1345 (2003).
20. The band depth D is determined by $D(\lambda) = 1 - R(\lambda)/[R(3.70) + R(2.35)]$ where R is the observed reflectance value at a given wavelength λ (μm). The integrated band depth is then calculated by integrating the band depth for each λ between 2.9 and 3.7 μm.
21. J.-P. Bibring, S. Erard, *Space Sci. Rev.* **96**, 293 (2001).
22. A. Gendrin *et al.*, *Science* **307**, 1587 (2005); published online 17 February 2005 (10.1126/science.1109087).
23. R. E. Arvidson *et al.*, *Science* **307**, 1591 (2005); published online 17 February 2005 (10.1126/science.1109509).
24. Y. Langevin, F. Poulet, J.-P. Bibring, B. Gondel, *Science* **307**, 1584 (2005); published online 17 February 2005 (10.1126/science.1109091).
25. S. W. Ruff *et al.*, *J. Geophys. Res.* **106**, 23921 (2001).
26. R. E. Arvidson *et al.*, *J. Geophys. Res.* **108** (E12), 8073 (2003).
27. D. T. Vaniman *et al.*, *Nature* **431**, 663 (2004).
28. Olivine weathering to sulfates has been discussed in the framework of acid fog (*30–32*).
29. J. Laskar *et al.*, *Icarus* **170**, 343 (2004).
30. M. Settle, *J. Geophys. Res.* **84**, 8343 (1979).
31. A. Banin *et al.*, *J. Geophys. Res.* **102**, 13341 (1997).
32. N. J. Tosca *et al.*, *J. Geophys. Res.* **109**, 10.1029/2003JE002218 (2004).

33. The OMEGA instrument has been developed with the support of Centre National d'Etudes Spatiales (CNES), Agonzia Spatiale Italiana (ASI), and Russian Space Agency. The scientific activity is funded by national space and research agencies and universities in France, Italy, Russia, Germany, and the United States of America. We are very grateful to the entire ESA teams who, together with industry, enabled this mission. We thank G. Neukum and the High Resolution Stereo Camera (HRSC) team who provided us with images of areas mapped by OMEGA. Vassili I. Moroz (Fig. 9) was a member of the OMEGA team until he passed away 23 June 2004. He was a pioneering planetologist who provided an outstanding contribution to OMEGA. This paper is dedicated to him.

16 December 2004; accepted 8 February 2005
Published online 17 February 2005;
10.1126/science.1108806
Include this information when citing this paper.

REPORT

Summer Evolution of the North Polar Cap of Mars as Observed by OMEGA/Mars Express

Y. Langevin,[1]* F. Poulet,[1] J.-P. Bibring,[1] B. Schmitt,[2] S. Douté,[2] B. Gondet[1]

The Observatoire pour la Minéralogie, l'Eau, les Glaces, et l'Activité (OMEGA) visible-infrared imaging spectrometer extensively observed regions of Mars with latitudes above 70°N in late 2004 (heliocentric longitude from L_s 93° to L_s 127°). The extent of water ice at the surface and the size of ice grains were monitored as a function of time. Bright, small-grained frost, which initially covered a large fraction of the polar cap, waned in favor of large-grained ice. In outlying regions, dominated by large-grained ice, the albedo increased over the period. Evaluating the dust content was model dependent. However, contamination of ice by dust was low.

The permanent caps of Mars were first comprehensively observed by Viking in 1976. Thermal infrared (IR) observations by Viking and then Mars Global Surveyor (MGS) Thermal Emission Spectrometer (TES) demonstrated that the surface of the permanent north polar cap is dominated by water ice (*1*, *2*). Analyses of imaging data from Mariner 9, Viking (*3*), and MGS (*4–6*) have demonstrated that the albedo of the north circumpolar regions varies within a single summer season and from summer to summer. Water ice is very bright in the visible spectrum when clean, but even a small amount of dust contamination can reduce the albedo to values close to that of the dust itself if the dust grains are embedded in ice grains (*7*). Determining

[1]Institut d'Astrophysique Spatiale, CNRS–Université Paris Sud, 91405 Orsay, France. [2]Laboratoire de Planétologie de Grenoble, CNRS–Université Joseph Fourier, 38400 Grenoble, France.

*To whom correspondence should be addressed. E-mail: yves.langevin@ias.u-psud.fr

the extent of surface water ice from visible data alone is therefore not straightforward.

Northern regions of Mars at latitudes higher than 70°N could be extensively observed by the Mars Express orbiter in October to December 2004, after the summer solstice (heliocentric longitude from L_s 93° to L_s 127°; Sun elevations ranging from 35° to 22°). During this period, the OMEGA visible–near-infrared imaging spectrometer (1.2-mrad instantaneous field of view, 8.8° swath width) mapped these regions with a resolution of 2 to 5 km/pixel, a scale at which local slopes are only relevant for a few locations. The spectral range of OMEGA is 0.4 to 5.1 μm. The spectral sampling is 14 nm, and the signal-to-noise ratio exceeds 300 from 1.1 to 2.6 μm (*8*, *9*), a spectral range that covers the strong ice bands at 1.5 and 2 μm (H_2O) and 1.43, 2, and 2.6 μm (CO_2). The calibration uncertainty on the photometric function is ~10% and that on broad-band strengths is ~3%. Reflectance and band-strength variations of <0.5% can be monitored. Therefore, OMEGA can identify surface ices without relying on albedo. Only water ice was observed at the surface after L_s 77° (*8*), in agreement with (*2*). The strength of water ice absorption features in the 1- to 2.6-μm range strongly depends on grain size (Fig. 1). The absorption at 1.25 μm increases faster with grain size than that at 1.5 or 2 μm. For large grains (~1 mm), the 2-μm feature is saturated, with a plateau from 1.9 to 2.15 μm. This makes it possible to monitor the extent and grain size evolution of water ice exposed on the surface both qualitatively with global maps and quantitatively by modeling the evolution of spectra for regions of interest.

Global maps were obtained by using a false-color scheme at three wavelengths (1.085, 1.242, and 1.51 μm). The red level (1.085 μm) is representative of the continuum, the blue level (1.51 μm) corresponds to a deep water ice band, and the green level (1.242 μm) corresponds to an ice band that is only strong for large grains (Fig. 1). Ice-poor regions have a similar albedo at all three wavelengths; hence, they show up as shades of gray. Small-grained surface ice (10 to 100 μm) shows up as yellow with this color scheme, because it has high albedos at 1.085 μm (red) and 1.25 μm (green), and a low albedo at 1.51 μm (blue). Large-grained surface ice (~1 mm) shows up as red in this color scheme, because it has a high albedo at 1.085 μm (red) and low albedos at 1.242 μm (green) and 1.51 μm (blue).

The first comprehensive coverage of circumpolar regions (Fig. 2) was obtained between 27 September and 8 October 2004 (L_s 93° to 98°). The distribution of surface water ice (red to yellow) is similar to that of the bright albedo features observed by Viking (*3*), except for a dent on the Olympia Planitia lobe. The smaller albedo notch at 205°E on this lobe observed by Mariner 9 (*3*) is similar to that in the OMEGA surface water ice map.

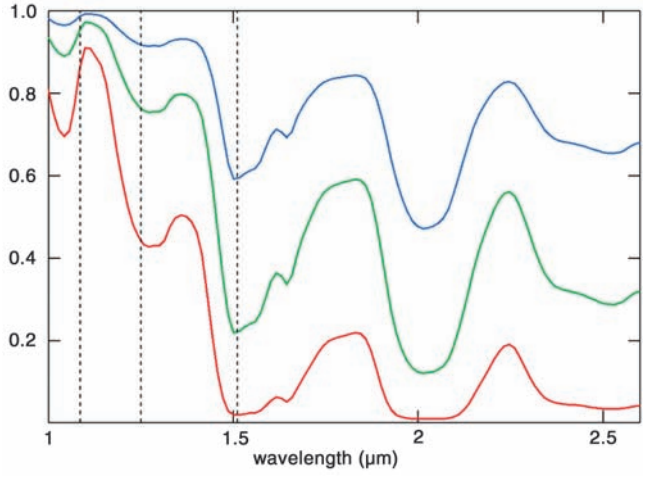

Fig. 1. Model spectra of pure water ice from 1 to 2.6 μm as a function of grain size calculated with a radiative transfer model (*10*). Blue: 10 μm; green: 100 μm; red: 1 mm. The dashed lines at 1.085, 1.242, and 1.51 μm correspond to the three OMEGA wavelengths that were used to monitor the evolution of grain size in the maps of Figs. 2 and 3.

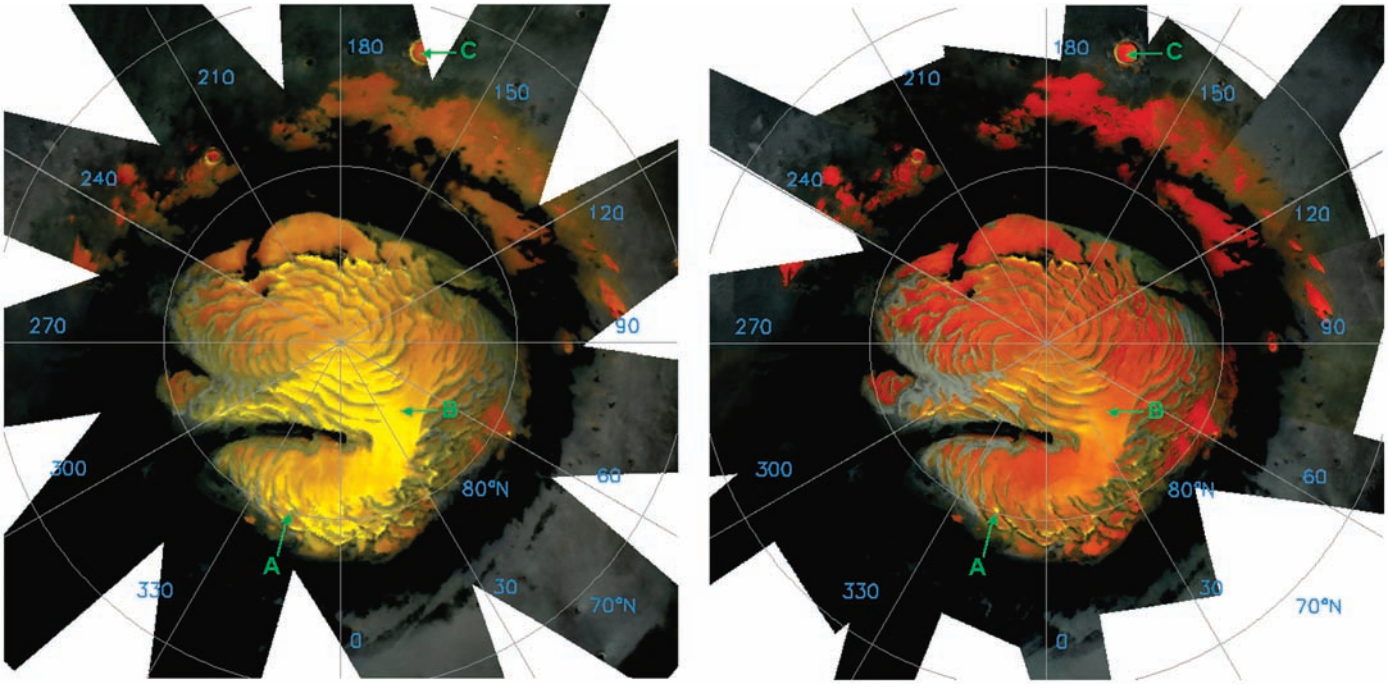

Fig. 2. (**Left**). RGB composite of 11 OMEGA tracks acquired between 27 September 2004 (L_s 93.3°) and 8 October 2004 (L_s 97.9°). Red color plane: Lambertian albedo at 1.085 μm; green color plane: Lambertian albedo at 1.242 μm; blue color plane: Lambertian albedo at 1.51 μm. For the each of the three color planes, the full scale (0 to 255) corresponds to an albedo range of 0.25 to 0.60. **Fig. 3** (**Right**). RGB composite of nine OMEGA tracks acquired between 29 October 2004 (L_s 107.4°) and 4 November 2004 (L_s 110.3°). The RGB color scheme is the same as in Fig. 2.

Nearly half of the ice-rich regions at latitudes higher than 80°N was then covered with bright fine-grained water ice (bright yellow). Absorption strengths at 1.24 and 1.51 μm in outlying regions correspond to those of large-grained ice with a dust contribution, because the albedo contrast is weak.

A second map (Fig. 3) was obtained between 29 October and 4 November 2004 (L_s 107° to 110°). The extent of regions with exposed water ice remained very stable over the 1-month interval since the map of Fig. 2 was obtained. However, only a few small areas at the edges of the central ice-rich region are still characterized by a small grain size (bright yellow). Most regions with exposed water ice are now dominated by large grains (red). This major evolution of the grain size of water ice exposed at the surface is associated with a decrease in albedo in the continuum for regions with latitudes higher than 80°N. The albedo contrast in the continuum between ice-rich areas at latitudes lower than 80°N and the surrounding dust-covered regions is much sharper in early November than in early October, with the same spatial distribution of surface ice. Therefore, the variations in ice coverage between different martian years that have been discussed on the basis of albedo contrasts (*3*–*6*) must be considered with caution.

Indeed, as previously reported (*7*, *10*), major albedo variations of surface ice can result from changes in grain size or from a dust contribution, with a complex interaction between these parameters. This contribution results from a combination of the following processes, which lower the apparent albedo of exposed surface ice and reduce the contrast of the water ice absorption bands.

(i) Aerosols lower the flux received by the surface (atmospheric extinction, which lowers the apparent albedo), while contributing part of the received signal by backscattering. (ii) Subpixel dust patches on the surface (areal mixing) contribute to the reflectance in proportion to their fractional coverage. (iii) An intimate mixture of dust and ice grains modifies the scattering properties of the surface layers (*11*, *12*). This can result from cosedimentation of dust and ice grains on preexisting ice. (iv) Very small quantities of dust grains ($\ll$1%) embedded within a water ice matrix (intramixture) strongly decrease the albedo of large-grained ice because they can absorb photons before their backscattering on grain boundaries (*7*). Such a situation can be expected for ice grains nucleated on dust seeds.

The contribution of aerosols could be assessed in early November, because it became possible with nadir pointing to observe the same area with two very different solar incidences. In particular, a region covered by bright dust at 159.7°E, 73°N was observed with solar incidences of 53.9° and 73.2°, corresponding to a factor of 2 in terms of the aerosol column density on the path of incoming solar photons. The resulting decrease in the apparent albedo at 1.085 μm was only ~3%. Therefore, atmospheric extinction by aerosols had only a minor impact on our observations at incidences lower than 60° in early November. The apparent albedo of dark areas at 1.085 μm was larger in early October than in early November (13% instead of 11.5%). This can be attributed to a 1.5% change of the aerosol backscattering contribution over 1 month, which has only a minor impact on the albedo of ice-rich regions (~50% in the continuum). Water ice absorptions lower than 10% were observed in dusty circumpolar deposits very close to surface ice; hence, ice in aerosols played a minor role in early summer, in agreement with TES observations (*2*).

The evolution of three regions of interest (A, B, and C in Figs. 2 and 3) was investigated in terms of grain size and dust content using a model (*12*) based on a radiative transfer approach (*13*). Regions A and B could be observed repeatedly until mid-December (L_s 127°). Region C, at a latitude of 73°, could only be observed until late October (L_s 107°). The size of water ice grains is well constrained, because absorption features are very strong (Fig. 1). However, previous modeling work (*12*) shows that the type of dust-ice mixing (areal mixture, intimate mixture, or intramixture) has a major influence on quantitative evaluations of the contribution of different components. We obtain an upper limit in terms of the volume fraction of dust in surface ice by first considering an intimate mixture of dust and ice grains, no surface dust patches, and no aerosol contribution.

Region A (343° E, 80.2°N) remained very bright from L_s 93° to L_s 127° (up to 70% albedo at 1.085 μm). The evolution of the observed spectra from 1 to 2.6 μm is shown on Fig. 4A. During this period of more than 2 months, the albedo at 1.085 μm slightly increased (from 0.65 to 0.7). The upper limit on the dust contamination lowered from ~3% to ~2% in volume with dark dust 5 μm in size in intimate mixture with ice grains. The best model fit is obtained with ice grain sizes lower than 200 μm, ice grains with sizes <50 μm constituting 80% of the volume. The slight reduction in contrast of the 1.65-μm feature, which is temperature dependent (*14*), is consistent with a temperature increasing from ~160 to ~210 K. Such a temperature evolution is within the range observed by TES at similar latitudes and values of L_s (*2*). The persistence of such bright patches at the edge of ice-rich regions over several months suggests that they may consist of thick accumulations of small water ice grains, equivalent to snow drifts.

Region B (42.5°E, 85.1°N) is typical of the evolution of the spectrum of permanent exposed ice on the northern ice cap (Fig. 4B). The initial spectrum (L_s 93.3°) is similar to

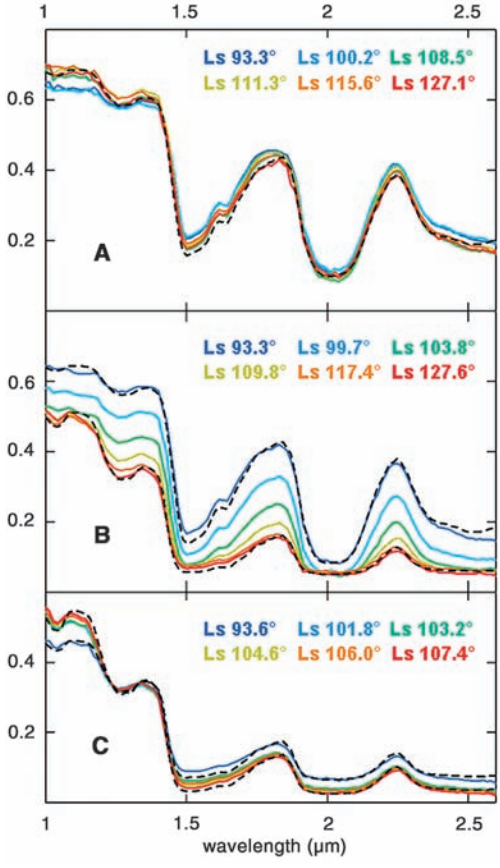

Fig. 4. Spectral evolution of regions of interest on the permanent cap at six values of L_s for each region. Each spectrum corresponds to the closest OMEGA pixel (2 to 5 km in size, depending on altitude), with a signal-to-noise ratio exceeding 300 from 1 to 2.6 μm. (**A**) 343°E, 80.2°N (region A in Fig. 3). (**B**) 42.5°E, 85.2°N (region B in Fig. 3). (**C**) 164.2°E, 72.4°N (Region C in Fig. 3); the spectrum at L_s 101.8° is mostly overlain by that at L_s 103.2°. The two dashed lines correspond to best-fit intimate mixture models for the initial spectrum (blue) and final spectrum (red). For region A, only the model spectrum corresponding to the final spectrum is drawn because there is no major evolution with time.

the initial spectrum of region A, dominated by ice grains in the sub–100 μm size range. The final spectrum (L_s 127.6°) is characterized by a lower albedo and a saturated 2-μm absorption feature, which corresponds to a much larger ice grain size. The best model fit is obtained when ice grains with a size of 700 to 800 μm constitute 70% of the volume. Ice metamorphism cannot explain such a size change in only 1 month (*7*). The most likely interpretation of this spectral evolution is therefore that fine-grained frost constituting the last remnants of the seasonal cap sublimates away, in agreement with models (*15*, *16*). This process exposes permanent ice, which is dominated by large grains (700 to 800 μm). This is similar to what is observed on terrestrial ice caps, such as Greenland, with a correlation between a decrease in albedo and the disappearance of seasonal frost (*17*). Dust contamination at the end of the period is 6% in terms of volume fraction, which is an upper limit because intimate mixture is assumed.

Region C lies within Korolev, one of the southernmost ice-filled craters, at a latitude of 73°N. From L_s 93.6° to L_s 107.4° (Fig. 4C), the spectra are characterized by a flat-bottomed absorption feature at 2 μm; hence, most of the volume (60 to 70%) is occupied by ice grains with sizes in the 700-μm to 1-mm range, similar to the final spectrum of region B. At L_s 93.6°, the observed spectrum has an albedo at 1.085 μm of 46% and an albedo at 2 μm of 6%; hence, the best model fit indicates an initial dust contamination (9% assuming intimate mixture) that is slightly larger than that in region B at the end of its evolution (6%). At L_s 107.4°, the albedo at 1.085 μm has increased to 52%, after which spectral evolution slows down. The albedo at 2 μm of the final spectrum is only 2.5%. Therefore, the upper limit of intimate dust contamination is low (<5%).

If part of the dust is embedded in the ice matrix (intramixture), spectral modeling of the observations leads to a negligible volume fraction of dust ($\ll$1% in all cases), in agreement with (*9*), and the estimated grain size remains the same as with the intimate mixture. If one also takes into account a possible contribution of aerosols, the conclusion is that the residual large-grained ice that is exposed since early summer in outlying regions and 1 month later on most of the ice cap itself is likely to be very clean. Either there is very little dust deposition during the global dust storm season (contrary to what is observed at lower latitudes) or there is an effective clean-up process during sublimation of the surface layers. The decrease in dust contribution that is observed between L_s 93° and L_s 107° in outlying regions (Fig. 4C) supports a surface clean-up process, even if a decrease in the optical thickness of aerosols cannot be totally excluded.

We have shown that in the central part of the north permanent cap of Mars, albedo variations in early summer are linked to a major increase in ice grain size, as seasonal frost with grain sizes <100 μm sublimates, so that the larger grains of the permanent ice (~1 mm) dominate the reflectance properties. In a few areas close to the edges of permanent surface ice regions, bright accumulations of small grains survive until late in the summer. In outlying ice-rich regions, the albedo markedly increases whereas the grain size (also ~1 mm) does not change. One month after the summer solstice, old ice is exposed at the surface over most ice-rich areas. This should lead to a net sublimation of ice with the present inclination. The low level of dust contamination of the ice remains to be explained, although there are indications that a clean-up process may be associated with sublimation.

References and Notes

1. H. H. Kieffer, S. C. Chase, T. Z. Martin, R. E. Miner, F. D. Palluconi, *Science* **194**, 1341 (1976).
2. H. H. Kieffer, T. N. Titus, *Icarus* **154**, 162 (2001).
3. D. S. Bass, K. E. Herkenhoff, D. E. Paige, *Icarus* **144**, 382 (2000).
4. P. B. James, B. A. Cantor, *Icarus* **154**, 131 (2001).
5. A. S. Hale, D. S. Bass, L. K. Tamppari, *Lunar Planet. Sci.* **34**, 1422 (2003).
6. M. C. Malin, K. S. Edgett, *J. Geophys. Res.* **106**, 23429 (2001).
7. H. H. Kieffer, *J. Geophys. Res.* **95**, 1481 (1990).
8. J.-P. Bibring *et al.*, *Science* **307**, 1576 (2005); published online 17 February 2005 (10.1126/science.1108806).
9. The visible part of the range would be useful for constraining surface dust content and composition. However, the visible channel (0.4 to 1 μm) still has some calibration problems, and atmospheric aerosols have a major influence at short wavelengths.
10. W. M. Calvin, T. N. Titus, *Lunar. Planet. Sci.* **35**, 1455 (2004).
11. S. Douté, B. Schmitt, *J. Geophys. Res.* **103**, 31367 (1998).
12. F. Poulet, J. N. Cuzzi, D. P. Cruikshank, T. Roush, C. M. Dalle Ore, *Icarus* **160**, 313 (2002).
13. Y. Shkuratov, L. Starukhina, H. Hoffmann, G. Arnold, *Icarus* **137**, 235 (1999).
14. W. M. Grundy, B. Schmitt, *J. Geophys. Res.* **103**, 25809 (1998).
15. M. A. Mischna, M. I. Richardson, R. J. Wilson, D. J. McCLeese, *J. Geophys. Res.* **108**, 5062 (2003).
16. B. Levrard, F. Forget, F. Montmessin, J. Laskar, *Nature* **431**, 1072 (2004).
17. A. W. Nolin, *J. Geophys. Res.* **103**, 25851 (1998).
18. This work was supported by CNES, CNRS, and Université Paris XI.

5 January 2005; accepted 7 February 2005
Published online 17 February 2005;
10.1126/science.1109438
Include this information when citing this paper.

REPORT

Sulfates in the North Polar Region of Mars Detected by OMEGA/Mars Express

Yves Langevin,* François Poulet, Jean-Pierre Bibring, Brigitte Gondet

The Observatoire pour la Minéralogie, l'Eau, les Glaces, et l'Activité (OMEGA) imaging spectrometer observed the northern circumpolar regions of Mars at a resolution of a few kilometers. An extended region at 240°E, 85°N, with an area of 60 kilometers by 200 kilometers, exhibits absorptions at wavelengths of 1.45, 1.75, 1.94, 2.22, 2.26, and 2.48 micrometers. These signatures can be unambiguously attributed to calcium-rich sulfates, most likely gypsum. This region corresponds to the dark longitudinal dunes of Olympia Planitia. These observations reveal that water alteration played a major role in the formation of the constituting minerals of northern circumpolar terrains.

The northern circumpolar regions of Mars constitute a complex geological region. Permanent ice deposits partially cover a bulge attributed to a water ice cap, as well as some low-altitude outlying regions down to latitudes of ~70°N. Intermixed with these bright areas, layered terrains and dark circumpolar sand deposits are observed. This entire region is a young complex system of layered deposits of ice and dust, plains, and dunes (*1*). The role of liquid water in the origin of these complex structures has been debated, either as outflows (*2*) or as large standing bodies of water (*3*, *4*). Mineralogical information is needed to constrain the geological history of these regions. Few unambiguous signatures have been observed in the northern circumpolar regions

Institut d'Astrophysique Spatiale (IAS), Bâtiment 121, 91405 Orsay Campus, France.

*To whom correspondence should be addressed. E-mail: yves.langevin@ias.u-psud.fr